UT-ICEPP 04-03
November 2004

# Neutron sensitivity of thin gap chambers

H. Nanjo * T. Bando K. Hasuko M. Ishino T. Kobayashi
T. Takemoto S. Tsuno B. Ye [1]

*International Center for Elementary Particle Physics, University of Tokyo, Tokyo 113-0033, Japan*

**Abstract**

Thin gap chambers (TGC) will be used for triggering forward muons in the ATLAS detector for the LHC at CERN. A large amount of neutron background is foreseen in the ATLAS experiment. This paper describes the measurements of the neutron sensitivities (detection efficiencies) of the TGCs. The sensitivities of both small and real size TGCs to 2.5 and 14 MeV mono-energetic neutrons were measured. For a small size TGC, sensitivities of 0.032% and 0.10% were measured to 2.5 and 14 MeV neutrons, respectively, whereas for a real size TGC, sensitivities of 0.048% and 0.13% were measured. These measured values were in reasonably good agreement with the simulations based on the Geant4.

*Key words:* LHC,ATLAS,trigger,thin gap chamber,TGC,neutron,Geant4
*PACS:* 29.40.Cs

## 1 Introduction

The ATLAS detector [1] is one of the major detectors for the future 14 TeV proton collider, the Large Hadron Collider (LHC) at the European Organization for Nuclear Research (CERN). The event rate of the ATLAS experiment is expected to be 1 GHz [2] for the designed luminosity of the LHC – $10^{34}$ cm$^{-2}$ sec$^{-1}$. The event trigger is one of the important issues for the experiment. Thin gap chambers (TGC) [3] will be used for triggering forward muons in the ATLAS detector. The structure of TGCs is similar to that of multi-wire proportional chambers and their detection efficiency for minimum ionizing particles (MIP) is more than 99% within

* Corresponding author. Tel.: +81-3-3815-8384; fax: +81-3-3814-8806;
*Email address:* nanjyo@icepp.s.u-tokyo.ac.jp (H. Nanjo).
[1] On leave from USTC, Hefei, People's Republic of China.

a 25 ns time gate [4] (time duration of this time gate is referred to as "time jitter"), that satisfies the requirements of the ATLAS muon triggering.

A large amount of background radiation is predicted in the ATLAS experiment. In the installation area of the TGCs, neutrons and photons are the primary components of the background. This may induce a high counting rate in the TGCs, thereby affecting stable operation and causing false muon triggers or the chamber aging. In order to estimate such effects, the sensitivities of TGCs to such background particles must be measured.

The primary energy range in the case of the photon background ranges from 10 keV to 10 MeV according to simulation [5], where photons are primarily generated through the capture of thermal neutrons. The sensitivity was measured in the energy range from 20 keV to 1.8 MeV and was found to be less than 1% [6].

In the case of the neutron background, it originates from the interaction of primary hadrons with the materials of the ATLAS detector and accelerator elements. Its energy spectra ranges primarily from 0.025 eV to 1 GeV with a gentle peak around the 500 keV region obtained from the simulation [5]. Recoil nuclei or fragments from neutron reactions can produce hits in the TGC. Photons generated through neutron reactions can produce electrons that can also be the cause of hits in the TGC.

We performed the first measurements on the neutron sensitivity (detection efficiency) of TGCs for mono-energetic neutrons of 2.5 and 14 MeV. The results of the measurements were evaluated with a Monte Carlo simulation that was based on the Geant4 [7] and a good understanding of the TGC response to neutrons was obtained.

## 2 Real size TGC and small size TGC

In this measurement, two types of the TGCs were used to get a better understanding through comparing both results. One was a real size TGC, the structure and materials of which were identical to that of the TGCs that will be used in the ATLAS experiment. The other was a small size TGC that had a smaller and a simpler structure than the real size TGC. The structure of the real size TGC is described in [8]. The cross sections of both real and small size TGCs are shown in Fig. 1. The anodes are gold-plated tungsten wires – 50 $\mu$m in diameter – uniformly spaced at 1.8 mm. The gap between the anodes and the cathode is 1.4 mm. The cathode surface is made of a conductive layer of approximately 10 $\mu$m in thickness, which primarily comprises graphite and acrylic resin in order to achieve a surface resis-

a) real size TGC

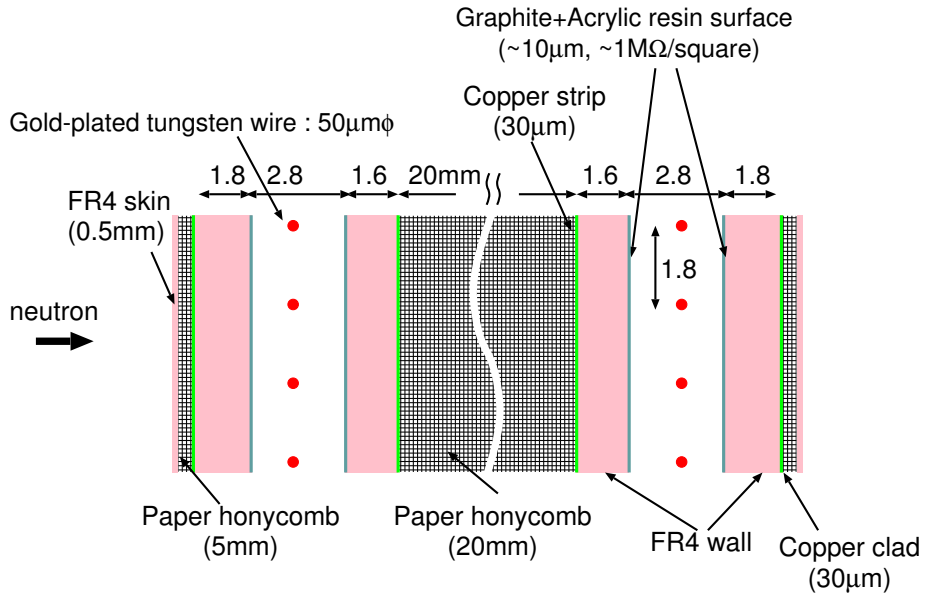


b) small size TGC

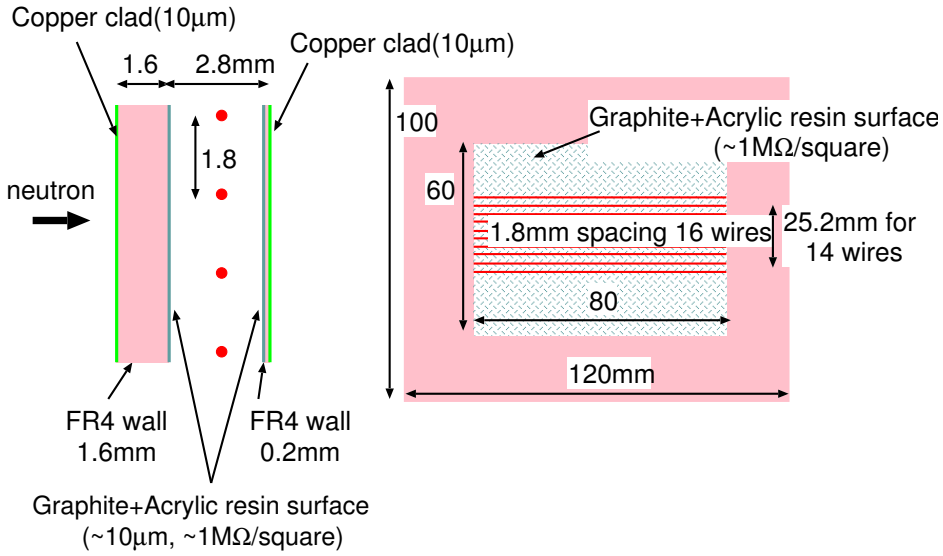


Fig. 1. The structure of the (a) real size TGC and (b) small size TGC.

tivity of approximately 1MΩ/square. The chamber walls are made of FR4 [2] . The TGC is operated in the limited proportional mode with a gas mixture of $CO_2$ and *n*-pentane, the ratio of which is 55 : 45.

The real size TGC is trapezoidal in shape – with a height of 1250mm and a base length of 1529mm. Approximately 20 wires are grouped together in order to obtain 32 channels for the anode readouts. There are 32 rows of copper strips, each with the thickness of 30 $\mu$m on the FR4 boards, which are perpendicular to the wires. Two chambers compose a double layer module (doublet) with a 20-mm thick paper

[2] flame retardant glass fabric base epoxy-resin laminate.

honeycomb between them to maintain mechanical rigidness. In addition, 5-mm thick paper honeycombs with 500-$\mu$m thick FR4 skins are glued on both the outer surfaces for protection and rigidness.

The small size TGC is 10 cm in width and 12 cm in length. It is a single layer chamber without cathode strip readouts. Its wire spacing, the wire diameter and the gap between the wire and the cathode are identical to that of the real size TGC. The thickness of one side of the chamber wall is 1.6 mm and that of the other side is 0.2 mm. The thickness of the copper cladding on the wall is 10 $\mu$m. There are 16 anode wires, each of which is 8 cm in length. The signals generated at each wire are individually read. The two edge wires are not used in order to eliminate the effect of a higher electric field and a larger drift space corresponding to the edge wires. Accordingly, the sensitive area was 8 cm in length and 2.52 cm in width.

## 3 Experimental setups

The geometrical and electrical setups for the measurements with both 2.5 MeV and 14 MeV neutrons are described in this section.

### *3.1 Experimental setup for the measurements of the sensitivities to 2.5 MeV neutrons*

Mono-energetic neutrons with energies of approximately 2.5 MeV were produced through d + D reactions [3] . A Cockcroft-Walton type accelerator in the Rikkyo University [4] was used to generate 97.5 keV $d^+$ ions. The ions were transported to a TiD [5] target, 0.5 mm in thickness, through a collimator (a 150-$\mu$m thick aluminum with a hole, the diameter of which was 6 mm). At the target, the mono-energetic neutrons with an energy of approximately 2.5 MeV were produced through a D(d,n)$^3$He reaction,

$$\mathrm{d} + \mathrm{D} \rightarrow \mathrm{n} + {}^3\mathrm{He} + 3.27\mathrm{MeV}.$$

Neutrons can be tagged with $^3$He nuclei generated at the same time. The geometrical setup around the target is shown in Fig. 2, where the x,y, and z coordinates are indicated. A Si PIN photodiode of 1 cm$^2$, S3590-02, fabricated by Hamamatsu Photonics, was placed at an angle of 90° with respect to the $d^+$ beam axis and at a distance of 14.5 cm from the target to detect $^3$He nuclei. A collimator of 500-$\mu$m

[3] D and d represent deuterium and deuteron, respectively.
[4] Rikkyo University 3-34-1 Nishi-Ikebukuro, Toshima, Tokyo 171-8501, Japan
[5] deuterium storage titanium.

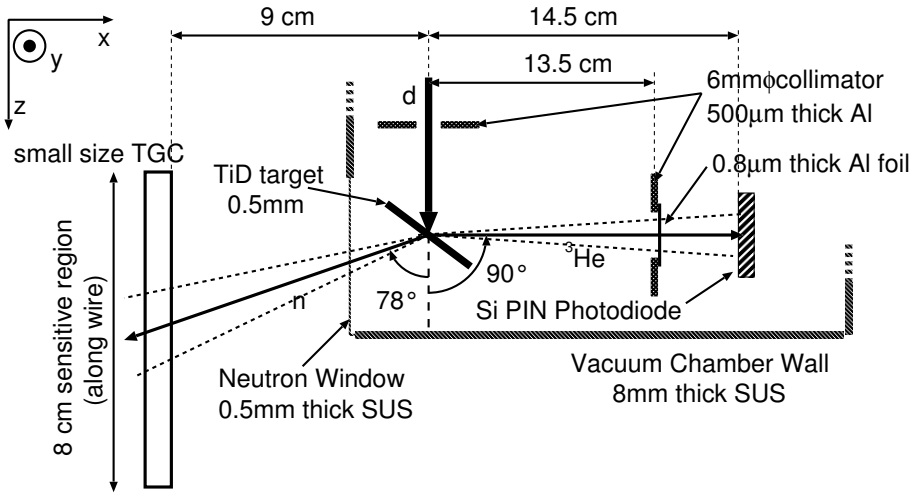


Fig. 2. The geometrical setup for the measurements of the sensitivities to 2.5 MeV neutrons. The small size TGC was placed at a distance of 9 cm from the target with its 1.6-mm thick FR4 wall near the target. The real size TGC was placed at a distance of 40 cm from the target.

thick aluminum with a hole 6 mm in diameter were placed in front of the photodiode. The collimator was positioned in order to define the direction of the $^3$He nuclei. A 0.8-$\mu$m thick aluminum foil was also positioned in front of the photodiode to stop deuterons coming from the target through Rutherford scattering in the target. All the apparatuses mentioned above were placed inside a vacuum chamber connected to the beam line.

When a $^3$He nucleon was detected at an angle of 90°, the energy of $^3$He nucleon was 800 keV and the corresponding neutron was emitted at an angle of 78° with its energy of 2.57 MeV in agreement with the two-body kinematics. Due to the energy loss of the deuteron in the target and the geometrical acceptance, the energy of the neutron ranged from 2.45 to 2.62 MeV at most. The full energy spread of the neutron was less than 7% and the emitting angle of the neutron in the x-z plane ranged from 93 to 65° at most.

There was a D(d,p)t reaction [6] besides D(d,n)$^3$He,

$$\mathrm{d} + \mathrm{D} \rightarrow \mathrm{p} + \mathrm{t} + 4.03\mathrm{MeV}.$$

According to the two-body kinematics, the proton energy was approximately 3.1 MeV whereas the triton energy was approximately 990 keV. Such protons and tritons could be rejected by applying cuts on the energy distribution measured with the photodiode. The photodiode energy calibration was performed using three types of $\alpha$ sources – $^{239}$Pu, $^{241}$Am, and $^{244}$Cm. The energy resolution of 0.2% around 5 MeV with a good linearity of 0.1% was obtained.

[6] t represents triton.

On the opposite side of the photodiode, a small size TGC was placed outside the vacuum chamber at a distance of 9 cm from the target, whereas a real size TGC was placed at a distance of 40cm from the target. The wall of the vacuum chamber was made of stainless steel (SUS) and was 8 mm in thickness. There was a 0.5-mm thick SUS neutron window at the side of the wall facing the TGC. From all the particles produced in the d + D reactions, only neutrons could enter the TGC, whereas the other particles were stopped at the vacuum chamber wall or the neutron window. The loss of the neutrons at the TiD target or the neutron window was negligible according to the Geant4 simulation and the loss was less than 5% according to the total cross sections. The TGC was set as its wires ran parallel to the z-axis and were spaced along the y-axis. The position of the TGC was designed such that it covered the cone of the neutrons corresponding to the $^3$He nuclei detected by the photodiode. Events due to the neutron incidence on the TGC (This implies that the neutron was emitted toward the TGC sensitive volume.) could be selected with a $^3$He hit on the photodiode. Events due to the neutron hit on the TGC (This implies that the neutron generated the hit signals of the TGC.) could be distinguished with the coincidence of a $^3$He hit at the photodiode and a hit on the TGC.

The electrical setup was designed to measure both the energy deposited in the photodiode with an peak hold ADC and time interval between the signal of the photodiode and that of the TGC with a TDC. The signal from the TGC was digitized with Amplifier-Shaper-Discriminators (ASD) [9] to supply the stop timing of the TDC. The signal from the photodiode was used for serving its charge, making the gate of the ADC and making the start timing of the TDC. In order to serve these functions, two amplifiers – shaping amplifier (SA) and timing filter amplifier (TFA) – were used after a pre-amplifier. The energy deposited in the photodiode was measured with the ADC using the signal from the SA. The coincidence timing was measured with the TDC which was begun by the signal from the TFA and halted by the signals from the TGC.

### *3.2 Experimental setup for the measurements of the sensitivities to 14 MeV neutron*

In the case of 14 MeV neutrons, mono-energetic neutrons were produced through the T(d,n)$^4$He reaction,

$$\mathrm{d} + \mathrm{T} \rightarrow \mathrm{n} + {}^4\mathrm{He} + 17.5\mathrm{MeV}.$$

There were no other d + T reactions except for the Rutherford scattering. The electrical setup was identical to that for the 2.5 MeV neutrons. The geometrical setup was slightly modified. A TiT [7] target, instead of a TiD target, was used. The T emit-

[7] tritium storage titanium.

ted 18.6 keV electron through beta decay. In order to avoid a high counting rate and pileups due to the beta rays, a 1-$\mu$m thick gold foil, instead of the 0.8 $\mu$m thick aluminum foil, was placed in front of the photodiode. It also stopped deuterons that were produced through Rutherford scattering. The 3.5-MeV $^4$He nuclei ($\alpha$ particles) were detected using the photodiode. The energy of the neutrons ranged from 14.0 to 14.2 MeV and the emitting angle of the neutrons ranged from 78 to 91° at most. The full energy spread was less than 2%.

## 4 Experimental results

Using the experimental setups described in the previous section, the measurements of the detection efficiencies to both 2.5 and 14 MeV neutrons were performed for both the small size TGC and the real size TGC. The analyses of the data are described separately for 2.5 and 14 MeV neutrons with the small size TGC, followed by the analysis with the real size TGC. The systematic uncertainties of the measurements are described in the last subsection.

### *4.1 Sensitivity of the small size TGC to 2.5 MeV neutrons*

The analysis for the sensitivity of the small size TGC to 2.5 MeV neutrons is described in this subsection. The energy distribution measured with the photodiode is shown in Fig. 3. Three peaks that corresponded to the 800 keV $^3$He nuclei, 990 keV triton, and 3.1 MeV proton are clearly seen. The decrease in their energy was primarily due to the energy loss in the 0.8-$\mu$m aluminum foil placed in front of the photodiode. Deuterons scattered in the target through Rutherford scattering were well stopped in the aluminum foil. In this energy distribution, events in the region from 100 to 700 keV were selected to obtain events with $^3$He detected by the photodiode. This selection was referred to as "loose $^3$He selection."

The timing distribution of the coincidence for the selected events is shown in Fig. 4 as an open histogram. The peak of the coincidence is clearly seen. The timing resolution of the photodiode mainly contributed to the width of the peak, while the "time jitter" of the TGC is 25 ns. In particular, the broadening of the peak in the 0 to 50 ns region in Fig. 4 was due to the time walk of the signals from the photodiode to start the TDC.

In Fig. 5, the energy distribution measured with the photodiode corresponding to the "loose $^3$He selection" is shown as an open histogram. The energy distribution for the events with a coincidence TDC from 0 to 400 ns is also shown as the hatched histogram. The ratio between them (coincidence ratio) is also plotted at the bottom. The decrease in the the coincidence ratio in an energy region around 250

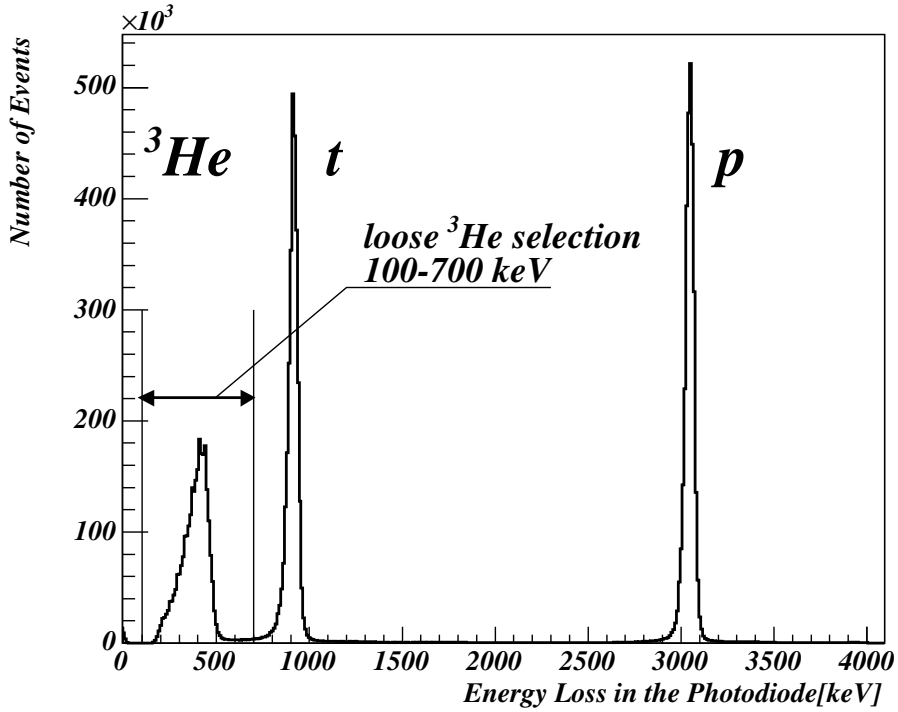


Fig. 3. The energy distribution measured with the Si PIN photodiode for the d + D reaction. The energy range corresponding to the "loose $^3$He selection" is indicated.

keV was due to the large time walk corresponding to the small $^3$He signals, which delayed the TDC start and the coincidence between the photodiode and the TGC was missed. In order to avoid such an effect, an energy region from 275 to 475 keV was selected for further analysis. This selection was referred to as "tight $^3$He selection." The number of events within the energy region for the open histogram was also referred to as $N_{\mathrm{neutron}}$, which implied the number of neutrons generated due to $^3$He nuclei detected with the photodiode.

The timing distribution for the events obtained with the "tight $^3$He selection" is shown as a hatched histogram in Fig. 4. The effect of the time walk was reduced with the tight energy selection.

The number of events within the region from 50 to 200 ns (coincidence region) in the distribution was referred to as $N_{\mathrm{coincidence}}$. The side bands for the distribution (The region of the former 50 ns and the latter 200 ns in Fig. 4.) were used to evaluate the accidental coincidence and the events in the side bands were fitted with a constant value. The fitted value was multiplied by the total bin number in the coincidence region to obtain the number of the accidental coincidences, $N_{\mathrm{accidental}}$.

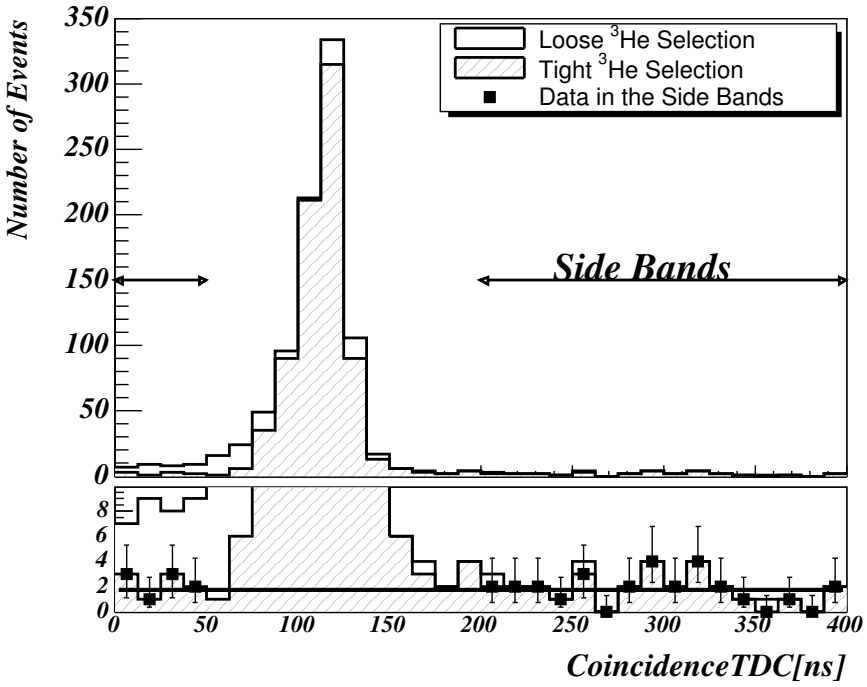


Fig. 4. The timing distributions of the coincidence within 400 ns. The open histogram corresponds to the events after "loose $^3$He selection" and the hatched histogram corresponds to the events after "tight $^3$He selection" that is indicated in Fig. 5. The lower regions of the histograms are magnified at the bottom. The "side bands" region (former 50 ns and the latter 200 ns) is indicated and the points with error bars correspond to events after "tight $^3$He selection" in the "side bands" regions. This was fitted with a constant value to estimate the accidental coincidence.

The detection efficiency was evaluated as follows.

$$\text{efficiency} \qquad = \frac{(N_{\text{coincidence}} - N_{\text{accidental}}) \times (1 - \xi_{\text{contamination}})}{N_{\text{neutron}}/(1 - \phi_{\text{loss}}) \times \eta_{\text{coverage}}}, \tag{1}$$

where $\phi_{\text{loss}}$ was defined as the loss of the neutron flux at the target or the neutron window, $\eta_{\text{coverage}}$ was defined as the TGC coverage for the neutron flux and $\xi_{\text{contamination}}$ was defined as the contamination of the hits of gammas in the coincidence region, which were produced through the reactions of the incident neutrons in the surrounding materials (The target chambers and concrete walls of the experimental area.).

The $\phi_{\text{loss}}$ was set to 0, as such loss was estimated to be negligible, as previously mentioned in subsection 3.1.

The hit wire distribution of the TGC was used for the estimation of $\eta_{\text{coverage}}$. The hit wire distribution, which corresponds to the events in the coincidence region is

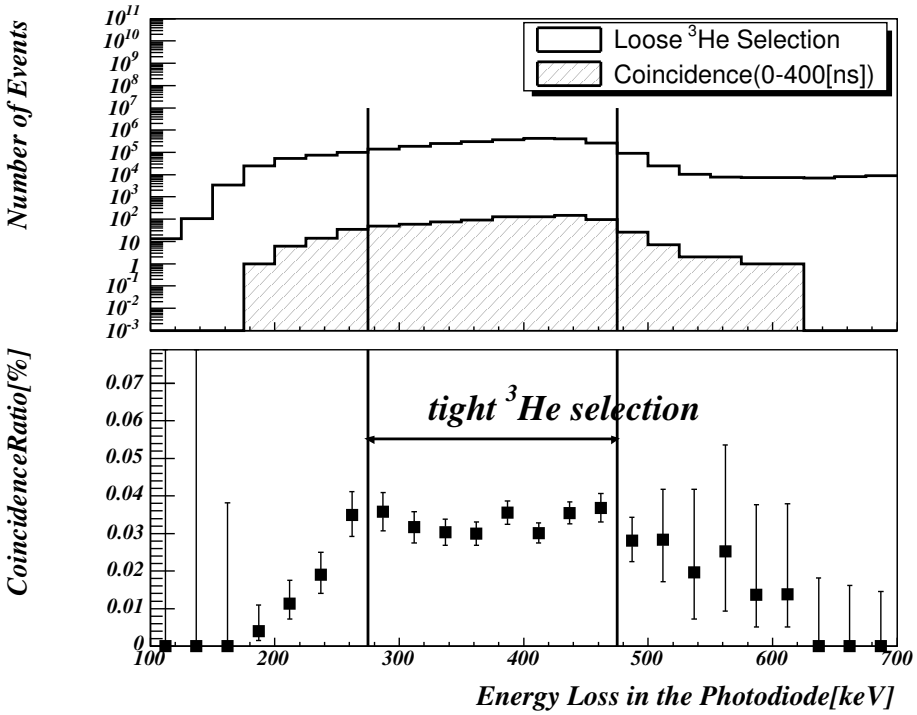


Fig. 5. The energy distributions measured with the photodiode for the events with the "loose $^3$He selection" (open histogram) and further with the coincidence within 400 ns (hatched one) are shown at the top. The coincidence ratio is also shown at the bottom. The energy range corresponding to the "tight $^3$He selection" is indicated.

shown in Fig. 6. The distribution was well restricted in the sensitive region which was 2.52 cm in width. This was confirmed by an analysis of other runs where the TGC was shifted to approximately $\pm$ 1 cm in the y direction as shown in Fig. 2. The distribution was fitted with a Gaussian plus constant value that was fixed at the value calculated from the number of accidental coincidences mentioned above. Subsequently, the coverage was estimated as being 99.4%. The other dimension of the sensitive area was 8 cm, which was wide enough to cover the entire neutron flux.

The $\xi_{\mathrm{contamination}}$ was estimated at 1.5% with the Geant4 simulation, where all materials (The target, target chamber, and concrete walls, where the concrete walls surrounding the experimental area were placed at a distance of approximately 1.5 m from the target.) were treated in addition to the TGC itself. The systematic uncertainties are discussed later in subsection 4.4.

The detection efficiency was calculated according to Eq. (1) and the result is shown in Table 1.

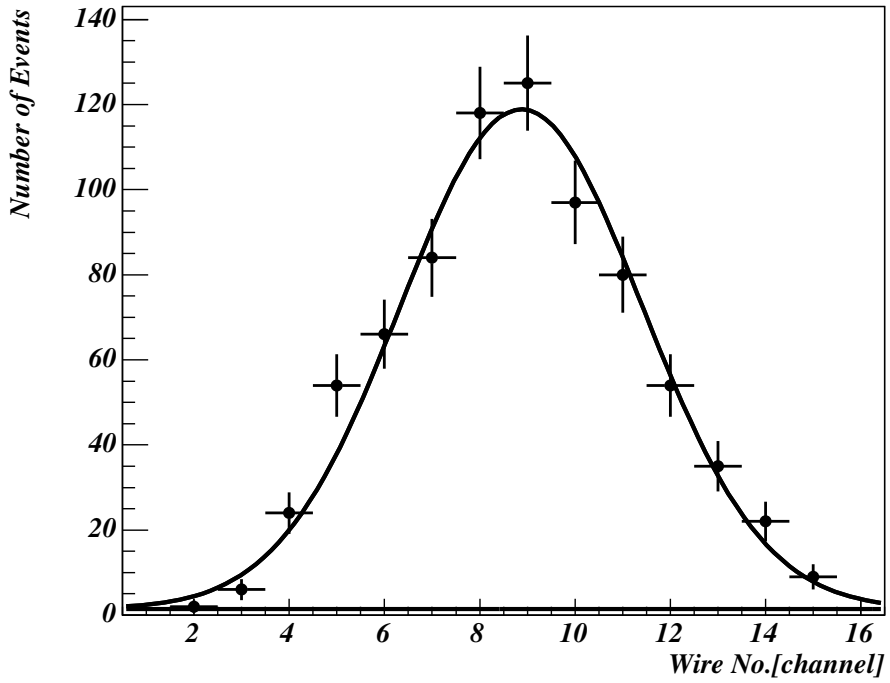


Fig. 6. The hit wire distribution of the TGC is shown. The distribution was fitted with Gaussian plus a constant value calculated from the event number of accidental coincidence. The width of sensitive area that corresponded to the 14 channels was 2.52 cm.

### *4.2 Sensitivity of the small size TGC to 14 MeV neutron*

The sensitivity of the small size TGC to 14 MeV neutrons was analyzed. The energy distribution measured with the photodiode corresponding to the d + T reaction is shown in Fig. 7. The peak corresponding to the 3.5 MeV $^4$He nuclei ($\alpha$ particles) is clearly seen. The decrease in the energy is primarily due to the energy loss in the 1-$\mu$m thick gold foil placed in front of the photodiode. Electrons from the tritium target through beta decay and deuterons scattered in the target through Rutherford scattering were well suppressed in the gold foil. The event selection in the case of 14 MeV neutrons was similar to that in the case of the 2.5 MeV neutrons. An event selection referred to as "loose $^4$He selection" entailed selecting the range of the energy distribution measured with the photodiode from 2.2 to 3.6 MeV, which is indicated in Fig. 7.

The energy distributions of events both after the "loose $^4$He selection" and with coincidence TDC from 0 to 400 ns is shown in Fig. 8. The ratio between them (coincidence ratio) is also shown at the bottom of the figure. The energy region from 2.9 to 3.2 MeV, where the coincidence ratio was stable was set as "tight $^4$He selection," which is indicated in Fig. 8.

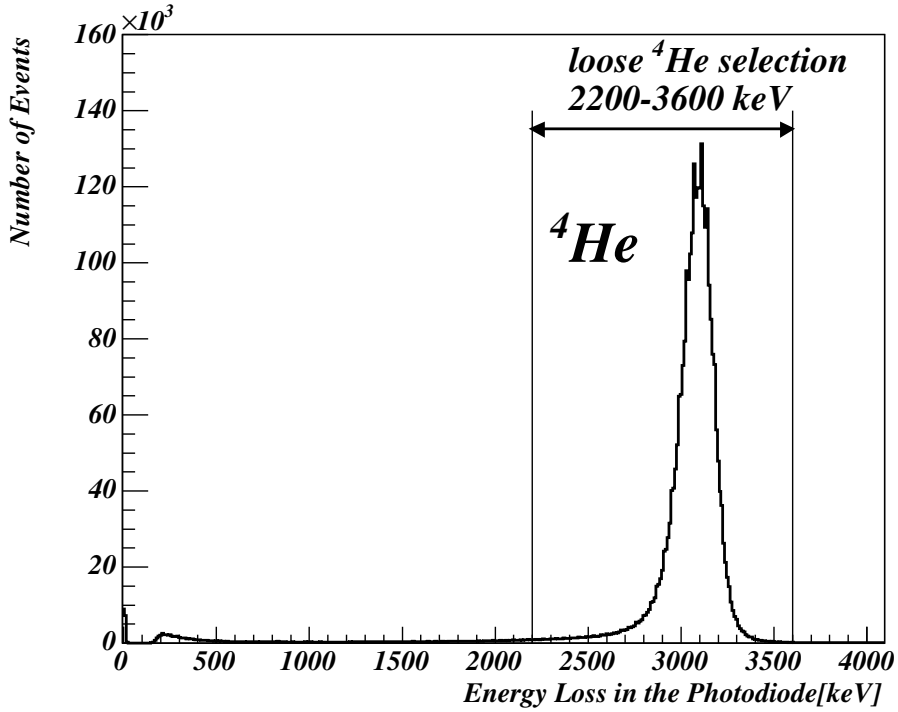


Fig. 7. The energy distribution measured with the photodiode for T(d,n)$^4$He reaction.

The timing distributions of the coincidence after the "loose $^4$He selection" and the "tight $^4$He selection" are shown in Fig. 9. The regions from 0 to 150 ns and 250 to 400 ns were referred to as "side bands." The points with error bars that corresponded to events after the "tight $^3$He selection" in the "side bands" were fitted with a constant value and the amount of accidental coincidence was evaluated.

The TGC coverage for the neutron flux ($\eta_{\mathrm{coverage}}$) was evaluated as 99.9% in a manner similar to that of the 2.5 MeV neutrons. The contamination of the hits of gammas in the coincidence region ($\xi_{\mathrm{contamination}}$) was evaluated as being 4% with the Geant4 simulation.

The result of the sensitivity for 14 MeV neutrons is also shown in Table 1. The evaluation of systematic errors was performed in subsection 4.4.

### *4.3 Sensitivity of the real size TGC*

The event selection for the analysis with the real size TGC was performed in a manner similar to that of the small size TGC except for the following three points.

The first is that a coincidence of the hits of the cathode strips was required in addition to that of the hits of the anode wires.

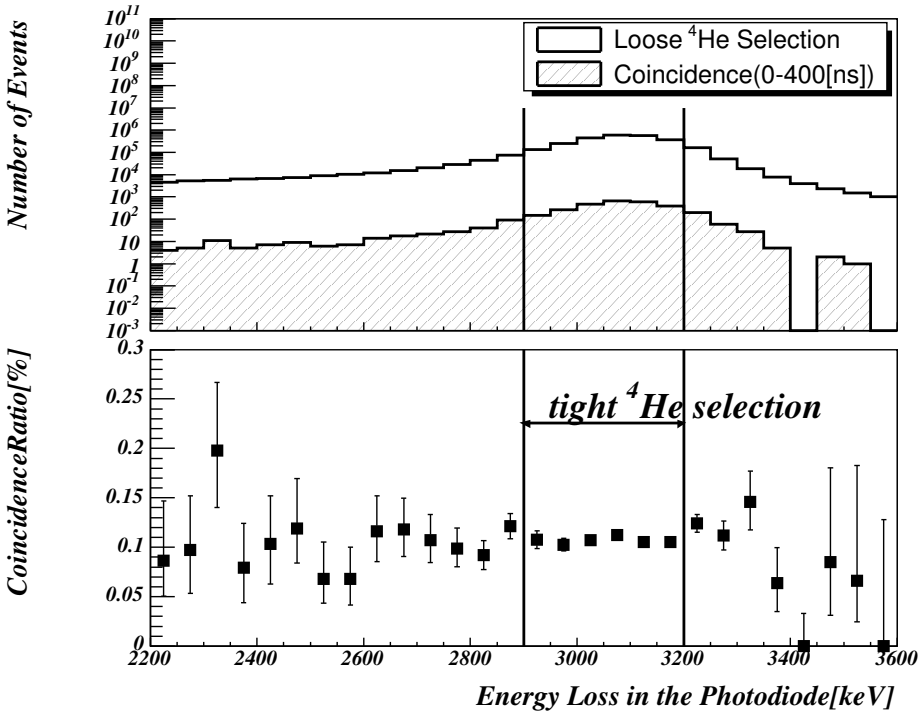


Fig. 8. The energy distributions measured with the photodiode for the events with the "loose $^4$He selection" (open histogram) and further with the coincidence within 400 ns (hatched one) are shown at the top. The coincidence ratio is also shown at the bottom. The energy range corresponding to the "tight $^4$He selection" is indicated.

The second is that the TGC hits within the area, 27 cm $\times$ 30 cm (7 channels in anode readouts $\times$ 7 channels in cathode readouts) were used as the neutron hits. This area was large enough to cover the neutron flux. The TGC coverage for the neutron flux was set to 100% for the real size TGC. This condition reduced the contamination of the hits by gammas produced in the surrounding materials.

The third is that the contamination of such gammas were evaluated with the data. The evaluation of the contamination for the case of 14 MeV neutrons is described below in detail. The measurement was performed with 15 anode readouts and 16 cathode readouts. The hit channel distribution after the "tight $^4$He selection" with TDC coincidence is shown in Fig. 10. With regard for the hit channel distribution, three regions were selected as follows. The first region was referred to as the "central region," which was a single bin with the largest bin contents. This is indicated as a region inside the dotted line in Fig. 10. The second region was referred to as the "inner region," where anode readouts from the 2nd to the 8th channel and cathode readouts from the 5th to the 12th channel were selected. This is indicated as a region inside the dashed line in Fig. 10. This region was used to calculate the center value of the neutron detection efficiency. The third region was referred to as the "outer region," which was outside the inner region. The contamination of gamma hits from the surrounding materials was smaller at the "central region" and was dominant at

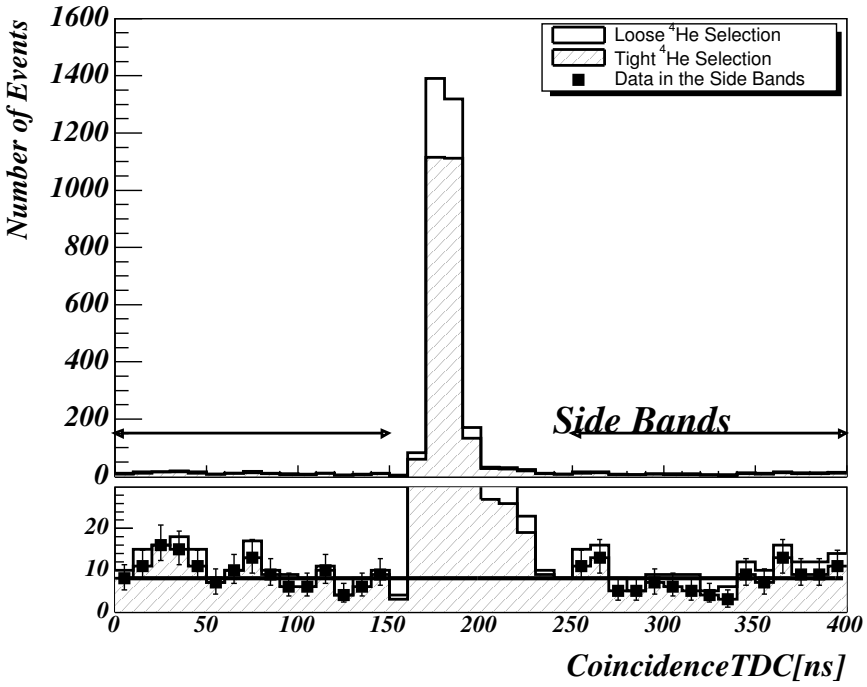


Fig. 9. The timing distribution of the coincidence after both the "loose $^4$He selection" (open histogram) and the "tight $^4$He selection" (hatched histogram). The points with error bars correspond to events after the "tight $^3$He selection" in the "side bands" regions (the regions from 0 to 150 ns and from 250 to 400 ns).

the "outer region" because the neutron flux was concentrated around the "central region." The timing distribution corresponding to the "inner region" was fitted with the shape of the two histograms, one corresponding to the "central region" and the other corresponding to the "outer region." The accidental coincidence, which was calculated in a similar manner as indicated in Fig. 4 was subtracted beforehand from each histogram. The result of the fitting is shown in Fig 11, where the contributions of both the central region and the outer region were indicated. The delay of the coincidence timing for the events in the "outer region" was primarily due to the time of flight of neutron to the concrete wall behind the TGC and the time for which the neutron existed in the wall. The gamma contamination in the timing distribution corresponding to the "inner region" was evaluated to as being $11 \pm 1\%$ according to the ratio of the contents of the two histograms used in the fit. With regard to this estimation, no contamination of such gamma hits in the "central region" and no contamination of neutron hits in the "outer region" were assumed and the possible contaminations were considered in the evaluation of the systematic errors in subsection 4.4. The estimation of the contamination according to the Geant4 simulation was 9%, where the target chambers and the concrete walls surrounding the experimental area were simulated. The gamma contamination for 2.5 MeV neutrons was evaluated in a similar manner as being $3 \pm 3\%$ and the estimation with the Geant4 simulation was 1%.

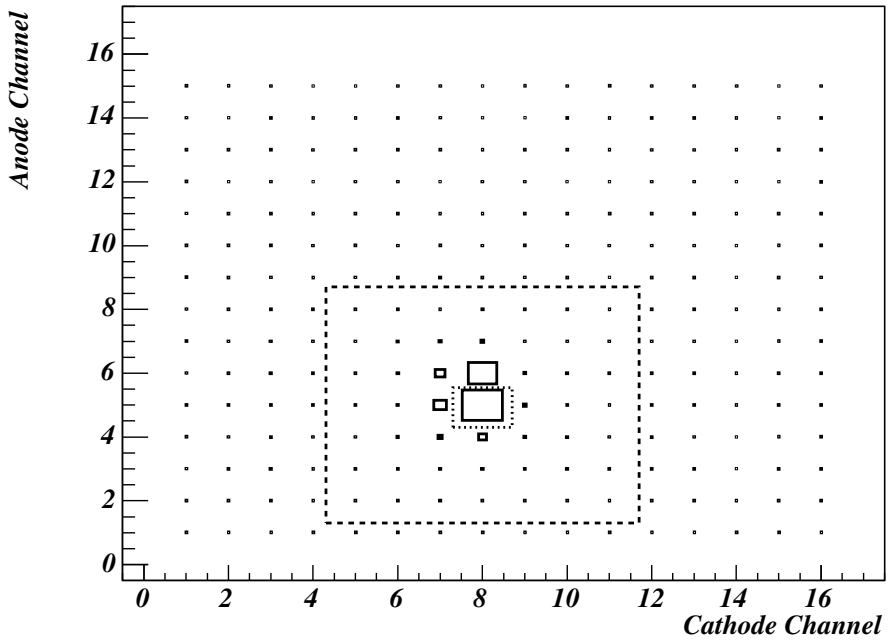


Fig. 10. The hit channel distribution after the "tight energy selection" with the TDC coincidence was plotted with boxes. A region inside the dotted line was referred to as "central region" and a region inside the dashed line was referred to as "inner region" and a region outside the "inner region" was referred to as "outer region."

The sensitivities of the real size TGC to 2.5 and 14 MeV neutrons were similarly calculated and the results are shown in Table 1.

Table 1
The measured sensitivities and the results of the simulation are summarized.

| | | Measurement | Simulation |
|---|---|---|---|
| small size | 2.5 MeV | $0.032 \pm 0.001(\text{stat})^{+0.003}_{-0.004}(\text{sys})[\%]$ | 0.035[%] |
| real size | 2.5 MeV | $0.048 \pm 0.001(\text{stat})^{+0.003}_{-0.005}(\text{sys})[\%]$ | 0.039[%] |
| small size | 14 MeV | $0.10 \pm 0.002(\text{stat})^{+0.01}_{-0.01}(\text{sys})[\%]$ | 0.11[%] |
| real size | 14 MeV | $0.13 \pm 0.002(\text{stat})^{+0.02}_{-0.02}(\text{sys})[\%]$ | 0.15[%] |

### *4.4 Systematic Uncertainties*

The systematic uncertainties for the sensitivities of both the small size and real size TGCs were evaluated in this subsection. As for Eq. (1), the systematic errors corresponding to the evaluations of $N_{\text{coincidence}}$, $N_{\text{accidental}}$, $\xi_{\text{contamination}}$, $\phi_{\text{loss}}$, and $\eta_{\text{coverage}}$ were considered.

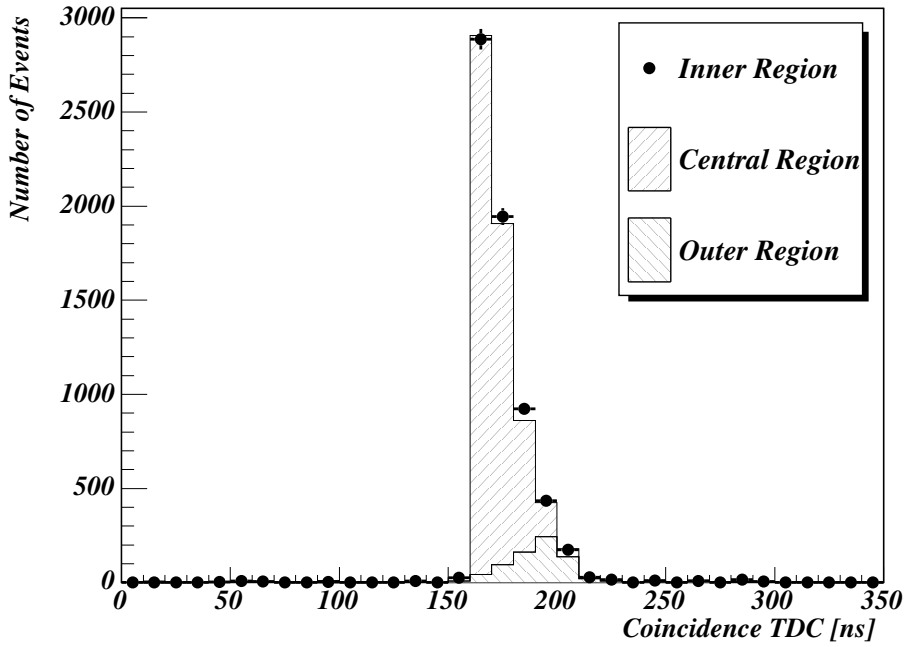


Fig. 11. The timing distribution after the "tight energy selection." The accidental coincidence was subtracted.

The "tight $^3$He/$^4$He selection" and the "side band" regions were altered to evaluate the systematic errors corresponding to $N_{\mathrm{coincidence}}$ and $N_{\mathrm{accidental}}$.

As for the evaluation of the $\phi_{\mathrm{loss}}$, the maximum loss of the neutron flux according to the total cross sections of the target and the neutron window was evaluated as being 5% and it was attributed to the systematic error.

The systematic error in the evaluation of $\eta_{\mathrm{coverage}}$ was considered only for the small size TGC. The amount of hits on the edge wires that were not included in the active area was used to estimate the maximum leak of the neutron flux and it was attributed to the systematic error.

Finally, the systematic uncertainties in evaluating $\xi_{\mathrm{contamination}}$ was considered. For the analysis with the real size TGC, $\xi_{\mathrm{contamination}}$ was evaluated with the assumption of the absence of the contamination of gamma hits in the "central region." The possible contamination of such gamma hits in the "central region" was estimated as being 10% using both the number of events in the "outer region" and a simulated distribution of the hit position of such gammas. The upper limit of $\xi_{\mathrm{contamination}}$ was set to 10% larger than the center value. The fluctuations of the sensitivities in modifying $\xi_{\mathrm{contamination}}$ from 0 to the upper limit was used at the systematic errors. The errors of the fitting to evaluate $\xi_{\mathrm{contamination}}$ were also considered.

For the analysis with the small size TGC, the sensitive area was approximately

1/100 as compared with that of the real size TGC, and the distance from the walls of the experimental area was greater than for the real size TGC. Accordingly, the effect of the contamination was considered to be smaller. However, an identical upper limit for the contamination as that for the real size TGC was conservatively assigned.

Among all the systematic errors, the systematic error due to the contamination of the coincident hits of gammas from surrounding materials had a major contribution. The experimental results with the systematic errors are shown in Table. 1 and in Fig. 12.

## 5 Simulation and discussion

In order to understand the above results, a Monte Carlo simulation based on the Geant4 was performed. For this simulation, all the geometrical configurations and materials of the TGC were implemented. The real size and small size TGCs were modeled separately and each anode wire was implemented. The incident angle of the neutron was set to $0^\circ$ (perpendicular to the TGC plane) and the incident position was uniformly distributed from a wire to its neighboring wire.

The hits on the TGC were created when charged particles moved in the gas and their energy deposited in the gas was more than 50 eV. A single electron in the gas is sufficient to register a hit for the TGC operated in the limited proportional mode. Accordingly, the latter condition was introduced to simulate the threshold of ionization. When the threshold value was varied from 0 to 200 eV, it did not change the results of the simulation in the energy range of neutrons from 1 to 20 MeV.

The measured sensitivities and the results of the simulations are summarized in Table 1 and shown in Fig. 12. As regard to the results of the simulation, there was an uncertainty of approximately 10 to 20% due to the limited knowledge of the ratio of the components of the cathode surface and the variations of both the thickness and the density of the material used in the cathode surface.

The measured values were found to be in reasonably good agreement with the simulation. The lower sensitivities of the small size TGC were due to its smaller volume and thiner wall. The neutrons scatted in the small size TGC could escape from its volume more easily than the neutrons scattered in the real size TGC.

Furthermore, the contributions of each material to the sensitivities were studied with the simulation. Over 75% of the hits were produced by hydrogen nuclei for the neutron energy from 2.5 to 20 MeV. (The contribution of the hydrogen nuclei for a 1 MeV neutron was 65%.) The remaining hits were primarily produced by carbon and oxygen nuclei. Such nuclei entered in the gas volume of the TGC through nuclear

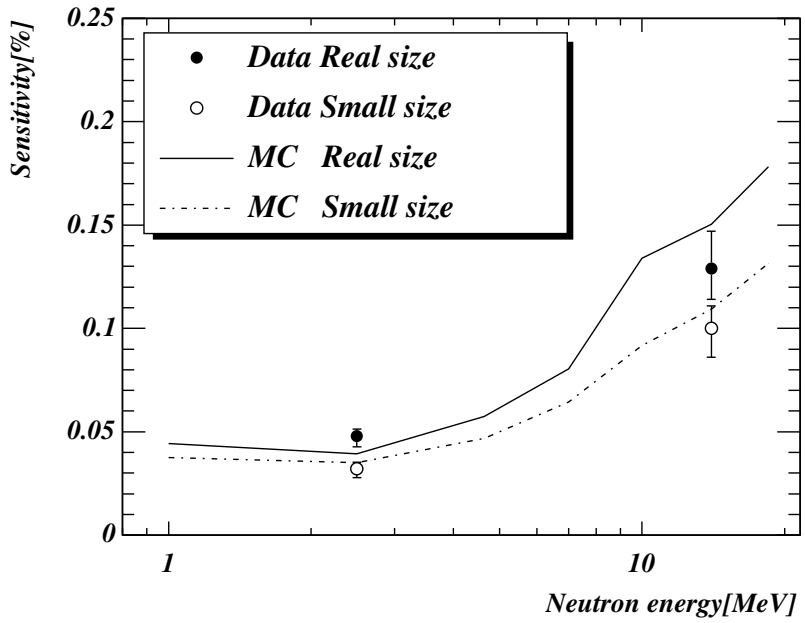


Fig. 12. Results of the sensitivities for the measurements and the simulations.

recoil by elastic scattering of the neutrons in each material. The contributions of each material to the sensitivity of the small size TGC are shown in Fig. 13, where the contributions from the copper and the wire are negligible and their markers are overlapped.

The contribution of the gas decreased as the neutron energy increased, which reflected mostly the cross section of the elastic scattering of the neutron. On the other hand, the contribution of the FR4 wall increased, which reflected the increase of the range of the recoil nuclei in the FR4 wall. The contribution of the cathode surface was saturated at the neutron energy above 2.5 MeV, where the range of a majority of the recoil proton exceeded the thickness of the cathode surface. However, the sensitivity decreased for the neutron energy in excess of 10 MeV, which was due to the decrease of the cross section.

Finally the dependence of the sensitivity on the incident angle of the neutron was studied with the simulation, which was important to estimate the rate of the neutron hits of the ATLAS experiment. The sensitivity increased as the incident angle $\theta$ (The angle between a line perpendicular to the TGC plane and the direction of the incident neutron.) increased. For the neutron energy of approximately 1 MeV, the sensitivity was approximately 1.1 times higher for $\theta = 30$ [deg], and approximately 1.4 times higher for $\theta = 45$ [deg], where the factor was approximately $1/cos\theta$. The gas made a major contribution to the sensitivity for such neutron energies, and the increase in the thickness of the gas due to the increase of the incident angle made a linear contribution to the increase in the sensitivity. As regards the neutron

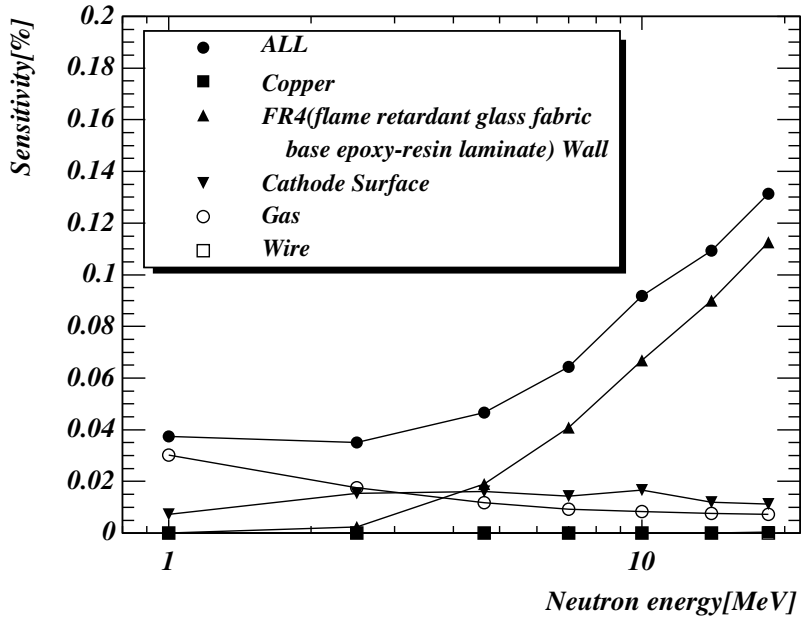


Fig. 13. The contributions of each material to the sensitivity are shown. The contributions from the copper and the wire are negligible and their markers are overlapped.

energy above 1 MeV, the sensitivities were 1-1.1 times higher for $\theta = 30$ [deg], and approximately 1.1 times higher for $\theta = 45$ [deg], where the decrease in the factor was due to the fact that the contributions of the FR4 wall and the cathode surface increased and the increase in the thickness for these materials did not make a linear contribution to the sensitivity. The thickness of the FR4 or the cathode surface beyond the range of the recoil nuclei did not contribute to the sensitivity.

## 6 Summary

The sensitivities of the TGC for 2.5 and 14 MeV mono-energetic neutrons were measured for both small and real size TGC. The Monte Carlo simulations based on the Geant4 were performed and the measured values were found to be in reasonably good agreement with those obtained from the simulation. Further studies with the simulations were performed and good understanding of the TGC response to neutrons was obtained.

## Acknowledgments

We would like to thank the members of ATLAS TGC group for supporting this work. We are also grateful for several types of assistance from the members of ATLAS-Japan TGC group. The real size TGC was constructed at the Institute of Particle and Nuclear Studies, High Energy Accelerator Organization (KEK). In particular, we would also like to thank the members of the nuclear and radiation physics laboratory in the Rikkyo University for supporting our measurements that were conducted there. They permitted us to use the Cockcroft-Walton type accelerator supported us in its operation and gave us valuable advice about the measurements.

## References

[1] ATLAS Technical Proposal, CERN/LHCC/94-43(LHCC/P2),1994.

[2] ATLAS Level-1 Trigger Technical Design Report, ATLAS-TDR12, 1998.

[3] S. Majewski, G. Charpak, A. Breskin, and G. Mikenberg, Nucl. Instrum. Meth. 217 (1983) 265.

[4] Y. Arai, *et al.*, Nucl. Instrum. Meth. A 367 (1995) 398.

[5] C. Battistoni, *et al.*,ATLAS Internal Note GEN-NO-010, 1994.

[6] S. Tsuno, T. Kobayashi, and B. Ye, Nucl. Instrum. Meth. A 482 (2002) 667.

[7] S. Agostinelli, *et al.*, Nucl. Instrum. Meth. A 506 (2003) 250.

[8] ATLAS Muon Spectrometer Technical Design Report, CERN/LHCC/97-22, 1997.

[9] O. Sasaki, *et al.*, IEEE Trans.Nucl.Sci.46 (1999) 1871.